From Nonlinear Dynamics to Trigonometry's Magic

From Nonlinear Dynamics to Trigonometry's Magic:

A Definite Vision of the Lorenz Equations

By

Belkacem Meziane

Cambridge Scholars Publishing

From Nonlinear Dynamics to Trigonometry's Magic:
A Definite Vision of the Lorenz Equations

By Belkacem Meziane

This book first published 2022

Cambridge Scholars Publishing

Lady Stephenson Library, Newcastle upon Tyne, NE6 2PA, UK

British Library Cataloguing in Publication Data
A catalogue record for this book is available from the British Library

ISBN (10): 1-5275-7763-5
ISBN (13): 978-1-5275-7763-3

To my wife, the cosine of my life

CONTENTS

PREFACE

Despite being the subject of intense research over the last four decades of the 20th century, the instability problem continues to lack a rigorous mathematical grounding. No analytical solution has been found to describe unstable systems, and these investigations have almost exclusively been concerned with convenient numerical algorithms [Lorenz 1963, Sparrow 1982, Robbins 1982, Fowler 1982], consequently obscuring the mathematics and physics correlating with nonlinear dynamics.

Among a variety of nonlinearly coupled differential equations to involve unstable solutions, the Lorenz-Haken set has undoubtedly drawn the greatest interest from scientists in physics and mathematics [Haken 1975, 1982]. Yet, at the end of the 1990s, after four decades of widespread attention, Stephen Smale - the 1966 Fields Medal laureate - had no option other than to slot the Lorenz attractor amongst a list of 18 challenging problems to be deferred to the 21st century [Smale 1998].

Let us recall that long before Smale's examination, various groups and individuals from distinct lines of thought had grappled with the instability issue, trying to reveal the hidden secrets of self-pulsing and deterministic disorder. Limiting this "history" to the field of laser physics, these include i) Hermann Haken, one of the leading theoreticians in the field of lasers and laser dynamics [Haken 1975, 1982], ii) W. E. Lamb Jr, the 1955 Nobel prize-winner in physics, and his team [Lamb 1964, Hendow & Sargent III 1982, 1985], and iii) L. W. Casperson, an Amnon Yariv disciple on quantum electronics and optics [Yariv 1967, Casperson 1983, 1985]. Combined with the efforts of many others, each group put forward their own methodologies, backgrounds, and approaches to bring suitable descriptions to the unpredictable features associated with the instability issue. Computer analysis played the role of an ultimate arbiter to endorse and substantiate any new outcome.

Yet, despite countless publications devoted to nonlinear dynamics being published from the early 1960s to the late 1990s, Smale's probe justifiably pointed out the lack of rigorous mathematics and proofs to clarify the origin of aperiodicity. Such a shortage culminates in an obvious deficiency in terms of decidability, i.e., the impossibility of predicting the path of a

chaotic trajectory given the set of control-parameter digits that govern the dynamics of any nonlinear system. Leaving the exploration of the solution properties to computer algorithms leads quite often to roundabout corroborations in relation to the strange attractor's features and clarifications [Galias and Zgliczy´nski 1998].

After severe numerical saturation, culminating with the sensation of some dead-end getaway, the scientific community at large gave up its interest on the subject, convinced that there was no more to offer - in terms of physics and mathematics - to clarify the strange trajectories outputting from computers and algorithm flows.

On the other hand, aiming at uncovering new and stirring information, the author's efforts to bring analytical foundations to the Lorenz-Haken equations kept going on a quasi-permanent basis [Meziane 1998, 2007, 2016, 2019]. Even though genuine approaches - mainly based on numerical-solution structuring – were put forward, no attempt or analysis carried enough mathematical rigor to dissipate Smale's prevalent frustrations. Expectantly, the present book will!

Let us also recall that the standard laser equations describe the semi-classical atom-field interactions that take place inside a unidirectional ring cavity [Lamb 1964, Sargent et al. 1974]. In the case of a single mode homogeneously broadened (SMHB) system these transform, after adequate approximations, into a simple set of three non-linearly coupled differential equations; the so-called Laser-Lorenz (or Lorenz-Haken) equations [Haken 1975]. Despite their simplicity, these deliver a remarkably broad range of solutions, ranging from periodic to erratic time traces, in the unstable regime of operation. The details of the solutions can only be tracked with the help of numerical integration [Meziane 2009, Khanin 2006]. These aspects closely depend on the exact values of four parameters: three decay rates correlated with the interacting variables (electric field, population inversion and polarization) and an external pumping parameter, which transforms an initially absorbing material into an amplifying medium. The first parameters relate to the medium's characteristics and to the geometry of the cavity. Accordingly, the only factor that may be freely adjusted is the excitation level supplied by the peripheral source. It constitutes the exclusive control parameter of the laser. The system turns out to be unstable when the (fixed) decay rates satisfy the bad cavity condition (i.e., that the field relaxation rate exceeds the sum of the inversion and polarization decay rates) and the pump parameter is raised beyond a critical value, referred to as the second laser threshold, or equivalently, the instability threshold. To avoid confusion, the

first laser threshold refers to the level of excitation required to initiate coherent laser action. It is much lower than the instability threshold, in the case of an SMHB system.

This book is meant to analytically extract all possible solutions with soft and strong harmonic expansion procedures. Excluding the small window of chaotic comportment, we shall derive analytical solutions to any periodic signal, including subharmonic cascading.

The book is organized as follows. First, it presents a summary of the Laser-Lorenz equations in Chapter I, recalling the important steps of the standard linear stability analysis. The method provides the position of the second laser threshold, as well as the frequency of the transient signal that develops from the stationary state, following the application of soft perturbations. After recalling the hierarchy of a few typical phase-space trajectories, a complete diagram is constructed from the numerical solutions. In Chapter II, we give a comprehensive survey of the weak amplitude state and propose some general solutions that obtain for any value of the cavity decay rate. Chapter III focuses on the strong harmonic state. Analytical solutions are proposed for both the low and high cavity relaxation factors. Chapter IV proposes a high-order trigonometry method to obtain analytical solutions for cavity decay-rates that involve self-pulsing signals. Leaning on spectra structures, Chapter V gives a few hints with regards to the construction of any asymmetric trajectory, including subharmonic solutions. Chapter VI focuses on the chaotic state, with new clues of analysis. To better capture trajectory features in phase-space, we recall a few mathematical basics connected to the so-called Lissajous depictions in Chapter VII, focusing on a few experimental set-ups whose characteristics are described in terms of phase-space trajectories. Finally, Chapter VIII proposes a new model, in the form of two coupled nonlinear oscillators, which clarify, in simpler aspects, much of the Lorenz-Haken dynamics.

While covering extremely detailed material, every effort has been made to facilitate reading by non-specialists. Those familiar with nonlinear dynamics may skip the first introductory chapters and dive directly into those containing innovative findings.

To avoid any cumbersome reading, complex calculations are presented in separate appendixes.

In addition to enlightening a good part of the fifty-year-long questioning of the Lorenz-Haken dynamics, this book is essential to mastering high-order

trigonometry. It is at the reach of the curious and willing student in physics and mathematics, especially at the graduate level.

CHAPTER I

THE LORENZ-HAKEN NONLINEAR DYNAMICS

This chapter summarizes the main ingredients of the analysis of the Lorenz-Haken equations. After reviewing a few typical hierarchies of numerical solutions, we propose a complete diagram in which we localize all possible solutions with respect to one main control parameter, namely, the normalized cavity decay-rate.

1 - From Light-matter interactions in a SMHB Laser to the Lorenz-Haken model

Light-matter interactions inside a unidirectional ring cavity are described in terms of three first-order differential equations that couple a resonant electric laser field to an amplifying medium that is described in terms of two variables: the population inversion and the polarization of a two-level atomic structure. These equations derive according to some self-consistent analysis, first proposed by W. E. Lamb in 1964 [Lamb 1964, Sargent et al. 1974]. In basic and normalized form, these equations take the form [Haken 1975, 1985, Narducci et al. 1988]

$$\frac{dE(t)}{dt} = -\kappa\{E(t) + 2CP(t)\} \tag{1a}$$

$$\frac{dP(t)}{dt} = -P(t) + E(t)D(t) \tag{1b}$$

$$\frac{dD(t)}{dt} = -\gamma\{D(t) + 1 + E(t)P(t)\} \tag{1c}$$

where *E(t), P(t), D(t)* represent, respectively, the laser field-amplitude, the polarization, and the population inversion of the amplifying medium, κ and γ are the cavity decay-rate and the population relaxation rate, both scaled to the polarization relaxation-rate, and $2C$ is an excitation parameter

that quantifies the external pumping mechanism with respect to its level at the lasing threshold. There is no need to recall the full properties of these equations, since these have been the subject of numerous full and consistent papers as well as books and book chapters. Let us just mention that the transition point from stable to unstable operation is a Hopf-bifurcation of the sub-critical type [Sparrow 1982]. This means that the departure from the stable state extends along some transient time during which the signal evolves with small oscillations whose amplitude gradually grows before reaching the final long-term solution with stronger amplitudes.

The trajectory converges to such a long-term solution only if the initial perturbation is strong enough to overwhelm the soft sinusoidal evolution around the stable, steady state. We shall focus on this important issue (so far omitted in the Nonlinear Dynamics literature) in Chapter II.

a) The steady-state solutions

The stationary state corresponds to the case for which the derivatives in Eqs (1) are set equal to zero. The dependence of each variable on the excitation parameter 2C extracts easily as

$$E_0 = \pm\sqrt{2C-1} \quad (2a), \qquad P_0 = \mp\frac{\sqrt{2C-1}}{2C} \quad (2b), \qquad D_0 = -\frac{1}{2C} \quad (2c)$$

These solutions only exist beyond a critical value of the excitation parameter 2C. In other words, according to Eq. (2a), the system delivers some coherent-field output when 2C > 1, which corresponds to the first laser threshold, for which the output intensity is $I = E_0^2 = 2C - 1$.

Note the double values of both the electric field and polarization. This important feature will serve as a hint to clear-out a few out-of-sight properties of the chaotic solutions.

Beyond this first laser-threshold, the system delivers a stable output for a range of excitations extending up to a second critical value, termed the "second laser threshold". Beyond such an "instability threshold", whose value directly relates to those of the control parameters κ and γ, Eqs (1) become unstable, yielding unsteady solutions in the form of regular pulse trains or fully erratic time traces. The exact trails of these solutions only be

obtained with numerical routines, yet the limited attempts towards extracting some analytical solutions to describe regular pulse-structures have been quite successful [Meziane 2009].

Let us mention that apart from the steady state solution given in Eqs (2), in a strict mathematical sense, the following solutions also fit in with Eqs (1),

$E(t) = 0$ (3a), $P(t) = 0$ (3b), $D(t) = -1$ (3c)

At first sight, one cannot understand the importance of such solutions, which have never been considered in the Lorenz Dynamics literature. However, disregarding such a fixed-point attractor amounts to neglecting a significant property of the asymptotic dynamics towards which the system converges when the control parameter κ reaches its upper limit. This aspect will be dealt with in Chapter IV.

b) Standard Linear Stability Analysis

The well-known linear stability analysis (LSA) is rooted in the application of small perturbations to Eqs (1) to delimit the conditions under which the system becomes unstable, with respect to its control parameters κ, γ, and 2C. The method, dealt with in any textbook that focuses on laser theory and instabilities [e.g. Hillborn 1994, Haken 1985, Meziane 2009; see also Appendix F, Chap. VIII], consists of superimposing small departures to the stationary solutions (Eqs (2)). Each of the three interacting variables *E(t)*, *P(t)*, and *D(t)* is substituted with

$$X(t) = X_0 + \delta x(t) \tag{4a}$$

in Eqs (1), to obtain new equations, in terms of the small perturbations $\delta x(t)$. The investigations into the stability problem assumes solutions of the form

$$\delta x(t) = x_0 \exp(\lambda t) \tag{4b}$$

and seeks the conditions under which a Hopf bifurcation occurs, i.e., when $\lambda = i\omega$. Such an assumption merely amounts to supposing some small-amplitude harmonic solutions around the stationary state.

A straightforward handling yields [See Chap. VIII, Appendix A] a first expression for the second laser threshold in the form

$$2C_{2th} = 1 + \frac{(\kappa+1)(\kappa+1+\gamma)}{(\kappa-1-\gamma)} \quad (5)$$

and a second expression for the pulsation of the perturbed signal evolving around its stationary state at the instability threshold

$$\Delta_t = \sqrt{\frac{2\kappa\gamma(\kappa+1)}{\kappa-1-\gamma}} \quad (6)$$

From both relations (5) and (6) another condition that a given system must satisfy to fulfill an unsteady operation appears. This requirement, called the bad cavity condition, reads

$$\kappa > 1 + \gamma \quad (7)$$

This last relationship illustrates the need for the laser-field decay-rate to exceed the sum of the polarization and population inversion relaxation rates to expect unstable output signals from a Single Mode Homogeneously Broadened Laser system. Given an amplifying medium (with fixed relaxation rates), the field decay rate remains the sole adjustable parameter, since it relates to modifiable cavity length and mirror reflectivity.

c) From three to one control-parameter-structure

With respect to the three control-parameters κ, γ, and 2C, Eqs (1) deliver an infinite number of distinct solutions, making it impossible to predict in advance which type of solution to expect. However, leaning on an isomorphic model that translates the Lorenz equations into a single control-parameter structure allows for a much more comprehensive approach and appreciation of the interaction-mechanisms hiding behind the wealth of different types of trajectories that are the signature of Lorenz-Haken Dynamics [Meziane 2016].

The simplified isomorphic structure results from the identification of some recurrent properties that define a class of solution for the same κ/γ ratio. Furthermore, leaning on extensive numeric experiences, we also found that fixing the excitation parameter at the instability threshold does not

reduce the assortment of solutions typical of the original three control-parameter set.

Based on these elements, Eqs (1) convert into

$$\frac{1}{\eta}\frac{dE(t)}{dt} + E(t) = -2C_{th}(\eta)P(t) \tag{8a}$$

$$\frac{dP(t)}{dt} + P(t) = E(t)D(t) \tag{8b}$$

$$\frac{dD(t)}{dt} + \{D(t) + 1\} = -E(t)P(t) \tag{8c}$$

where

$$2C_{2th}(\eta) = \frac{\eta(\eta+4)}{(\eta-2)}, \tag{8d}$$

and

$$\eta = \kappa/\gamma \tag{8e}$$

Appendix A demonstrates such an isomorphism with a few typical examples.

2 - Typical solutions and trajectories for small η values ($\eta = 2_+$)

According to Eq. (8e), the bad cavity condition (7) transforms into $\eta > 2$. Therefore, theoretically, the range of η values extend from $\eta = 2_+$ to infinity. Accordingly, the variety of solutions is extremely vast. Nevertheless, limiting the analysis in terms of that lone control-parameter makes it a much easier task to undertake some systematic line of analysis, with the aim of extracting a detailed account of the Lorenz Dynamics, despite the theoretically infinite range of the control parameter values.

First, let us focus on a series of typical solutions obtained by increasing η, beginning with lower values. For the purpose of capturing the puzzling nature of Lorenz Dynamics, this calls for threefold illustrations; a) temporal time traces of the electric-field $E(t)$, knowing that the laser-output intensity simply scales as $E(t)^2$, b) the field spectrum, obtained

with a Fast Fourier Transform of the corresponding signal, and c) the phase-space portrait, represented on any of the three $\{X(t), Y(t)\}$ planes.

Starting from $\eta = 2_+$, the electric-field temporal time trace consists of regular oscillations around the temporal axis (Fig. 1a). The solution is not purely sinusoidal but contains, in addition to a dominant frequency f_0 , a third and a fifth harmonic components with decreasing amplitudes (Fig. 1b). The phase-space depiction in the $\{E(t), D(t)\}$ plot of (Fig.1c) follows a perfectly symmetric trajectory with respect to the electric field axis.

At this point, it is worth mentioning that the fundamental long-term frequency f_0 does not exactly connect with that conforming to Eq. (6). It is lower inside the whole range of control parameters: $f_0 < f_t = \Delta_t / 2\pi$. This important issue, called redshift or slowing down effect, will be clarified in Chap. II, Appendix C.

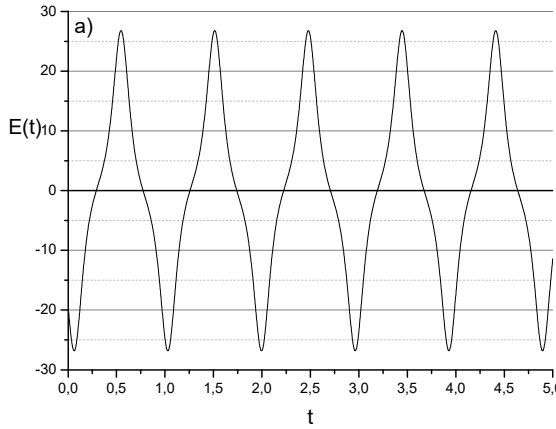

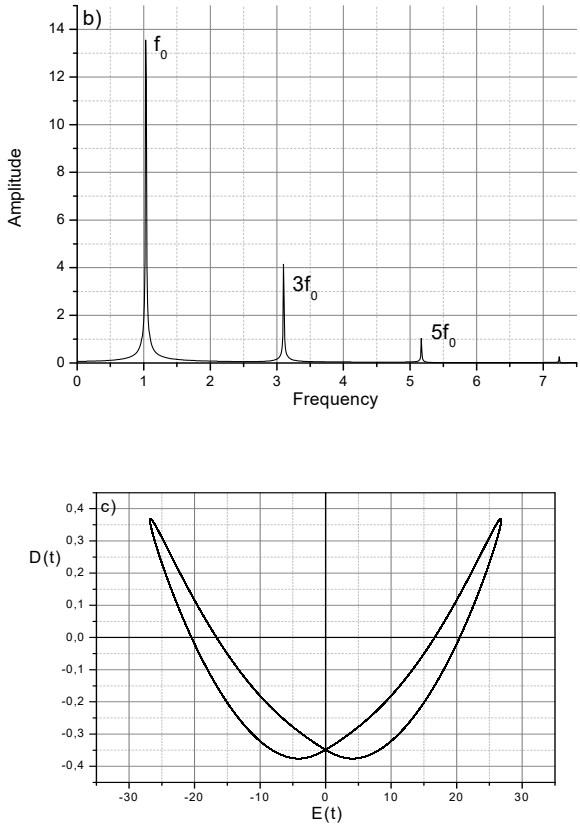

Figure 1 a) Electric field time-trace, b) Signal Fourier-transform, and c) Phase-space portrait obtained at η=2.05.

Increasing η from 2.05, to 2.1, Figs 1a-1c transform, respectively, into those of Figs 2a-2c.

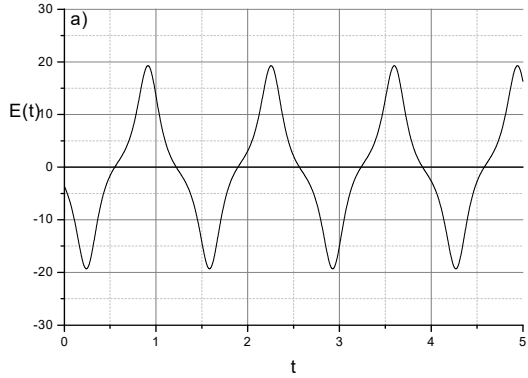
a)
E(t)
t
30
20
10
0
-10
-20
-30
0
1
2
3
4
5

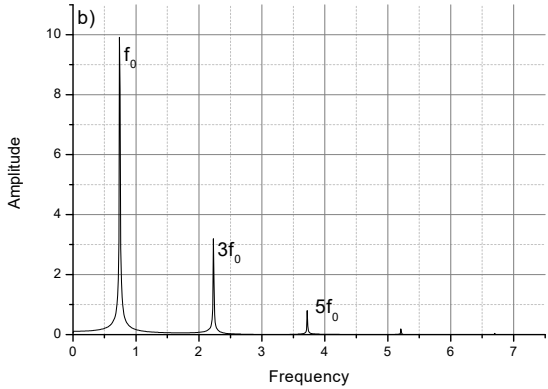
b)
Amplitude
Frequency
f0
3f0
5f0
10
8
6
4
2
0
0
1
2
3
4
5
6
7

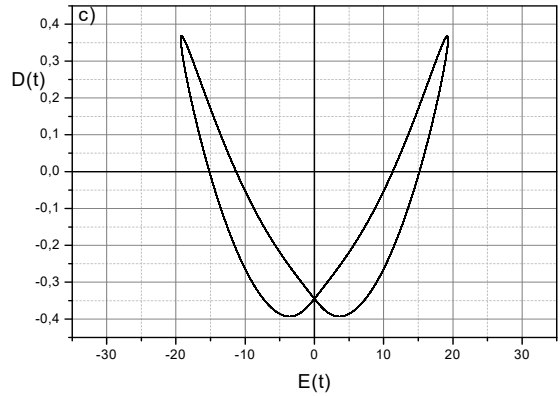

Figure 2 a) Electric field time-trace, b) Signal Fourier-transform, and c) Phase-space portrait obtained at η=2.1.

From first-glance comparisons, we notice an amplitude reduction of the electric-field amplitude, along with some shift towards lower frequencies of the corresponding spectrum. These modifications conform to the numerical variations undergone by the excitation parameter whose value is twice that of the first example. In terms of the steady-state fields and small-oscillation frequencies, $\eta = 2.05$ gives $E_0 \cong 15.71$ and $f_t \cong 2.52$, while $\eta = 2.1$ gives $E_0 \cong 11{,}27$ and $f_t \cong 1.82$. Therefore, these amplitude variations and frequency shifts are of no surprise. The phase-space trajectory remains symmetric, with the two branches getting closer, as expected from the field-amplitude reduction. Even though no obvious variations of $D(t)$ appear between Fig. 1c and Fig. 2c, a closer inspection reveals some tiny differences, mainly at the lower part of the curve. These variations are less obvious to perceive because the normalized population inversion variable scales in the limited range [-1, +1], while the electric field amplitude increases sensibly with increasing excitation.

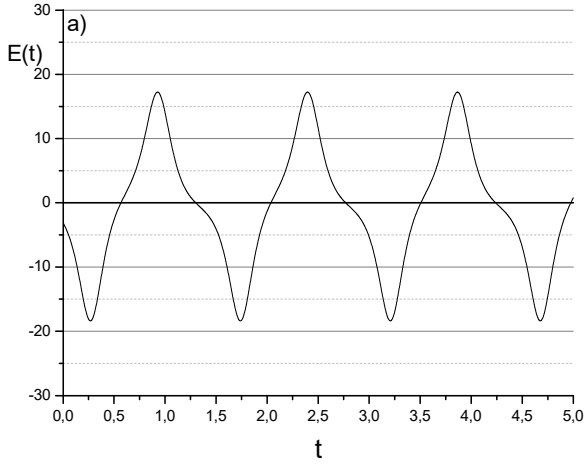
a)
E(t)
30
20
10
0
-10
-20
-30
0,0
0,5
1,0
1,5
2,0
2,5
3,0
3,5
4,0
4,5
5,0
t

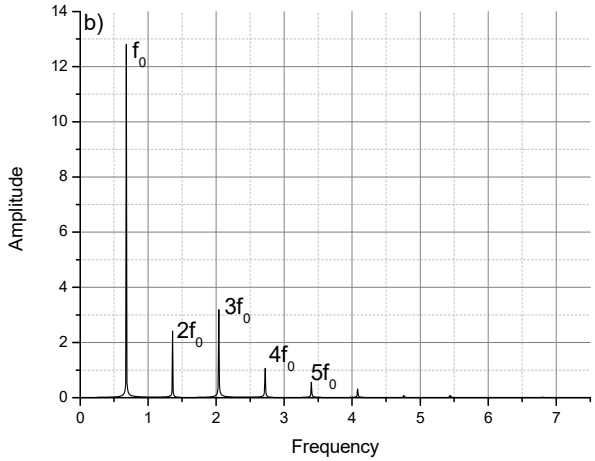
b)
Amplitude
f0
2f0
3f0
4f0
5f0
14
12
10
8
6
4
2
0
0
1
2
3
4
5
6
7
Frequency

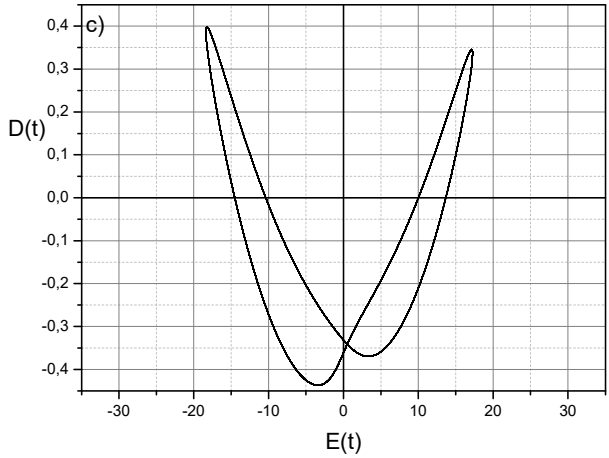

Figure 3 a) Electric field time-trace, b) Signal Fourier-transform, and c) Asymmetric phase-space portrait obtained with η = 2.12.

For $\eta = 2.12$, even though the electric-field lessens by only 9% with respect to that of Fig. 2 ($E_0 \cong 10{,}35$), drastic changes occur, both in the frequency spectrum, Fig. 3b, which shows additional even-harmonic-components, at $2f_0$, $4f_0$, and in the phase-space trajectory, Fig. 3c, which exhibits some noticeable symmetry-breaking, in the vicinity of the zero field values, as well as at the population inversion of left-and-right-branch peaks. These distortions go along the signal inharmonic distortions of Fig. 3a, transforming the period-one attractor of Figs 1c and 2c into the asymmetric orbit of Fig. 3c.

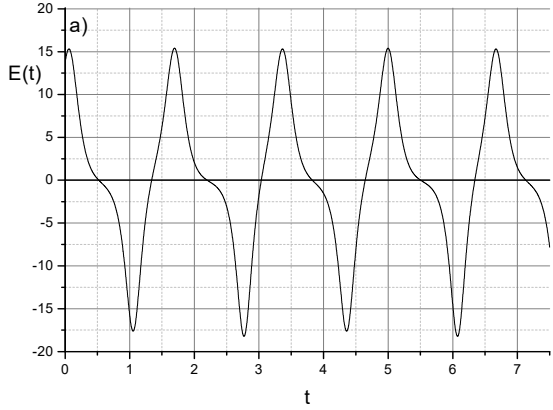
a)
E(t)
t
20
15
10
5
0
-5
-10
-15
-20
0
1
2
3
4
5
6
7

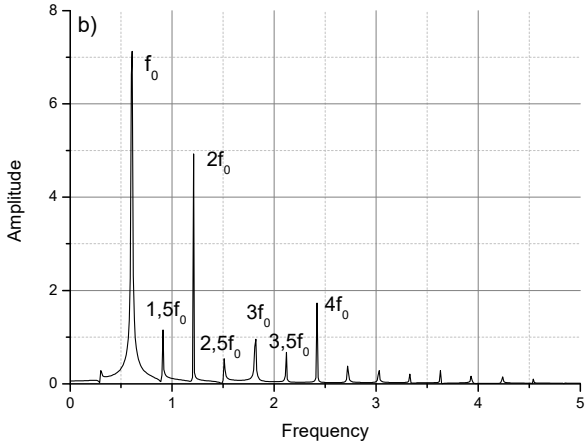
b)
Amplitude
Frequency
f0
2f0
1,5f0
2,5f0
3f0
3,5f0
4f0
8
6
4
2
0
0
1
2
3
4
5

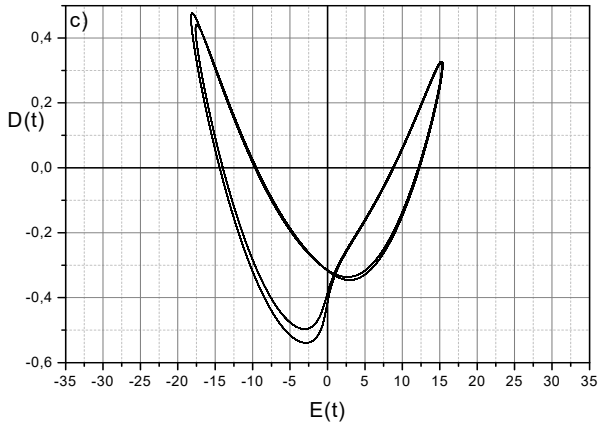

Figure 4 a) Electric-field time-trace, b) Signal Fourier-transform, and c) Double loop phase-space portrait obtained with η = 2.145.

For $\eta = 2.145$, with $E_0 \cong 9.48$ (the amplitude value of Fig. 3 again decreasing by 9%), close inspection of the electric signal, represented in Fig. 4a, reveals a regularly-occurring positive maximum amplitude, reaching $E_M \cong 15$, while the negative peaks alternate between $E_m \cong -17.5_+$ and $E_m \cong -17.5_-$. These variations signify the presence of additional modulating frequencies, as shown in the spectrum of Fig. 4b. In addition to those of Fig. 3b, a series of subharmonic components at $1.5f_0$, $2.5f_0$, $3.5f_0$, etc., arise between the even and odd ones. These additional frequencies convert the asymmetric single-loop phase-space trajectory of Fig. 3c, into a double-looped attractor, shown in Fig. 4c. The solution is designated as asymmetric period-two orbit.

For $\eta = 2.15$, $E_0 \cong 9.33$ (10% less than the preceding value), a first inspection of Fig. 5a reveals an almost identical signal to that of Fig. 4a. However, the corresponding spectrum, Fig. 5b, tells a different story. While the even frequencies persist, the odd and subharmonic components are masked inside some lower-amplitude continuum conforming to the chaotic multi-loop orbit of Fig. 5c. Note the pronounced asymmetry of the attractor as compared to that of the following case.

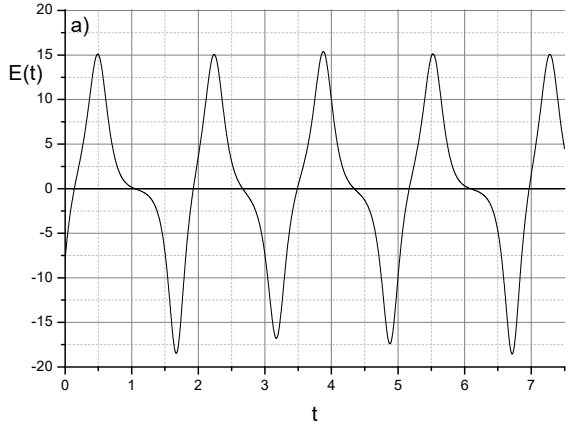
a)
E(t)
t
20
15
10
5
0
-5
-10
-15
-20
0
1
2
3
4
5
6
7

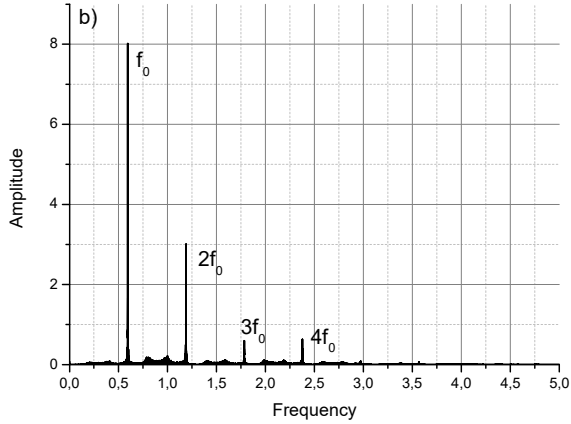
b)
Amplitude
Frequency
f0
2f0
3f0
4f0
8
6
4
2
0
0,0
0,5
1,0
1,5
2,0
2,5
3,0
3,5
4,0
4,5
5,0

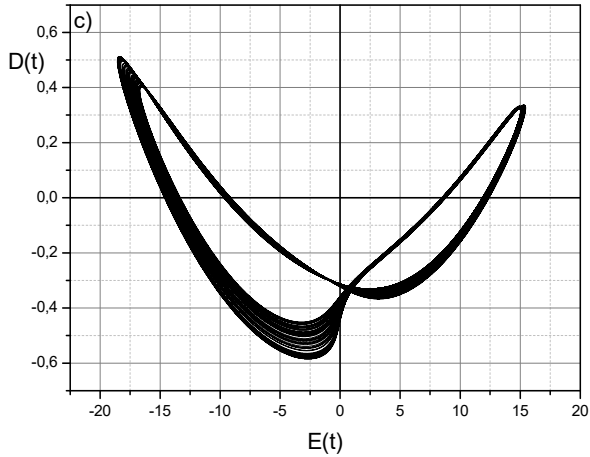

Figure 5 a) Electric-field time-trace, b) Signal Fourier-transform, and c) Phase-space portrait obtained with η = 2.15.

For $\eta = 2.16$, $E_0 \cong 9.06$ (again 10% less than the last value), the quasi-regular evolution of the previous examples breaks into an irregular time trace, as shown in Fig. 6a. The corresponding FFT, displayed in Fig. 6b, now consists of a broad spectrum, with the higher amplitudes packed in the vicinity of the fundamental frequency f_0 , and the phase-space portrait takes the form of a chaotic attractor with an almost symmetric structure as compared to Fig. 5c.

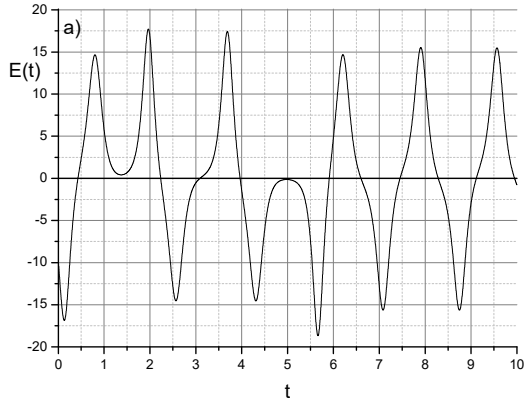
a)
E(t)
t
20
15
10
5
0
-5
-10
-15
-20
0
1
2
3
4
5
6
7
8
9
10

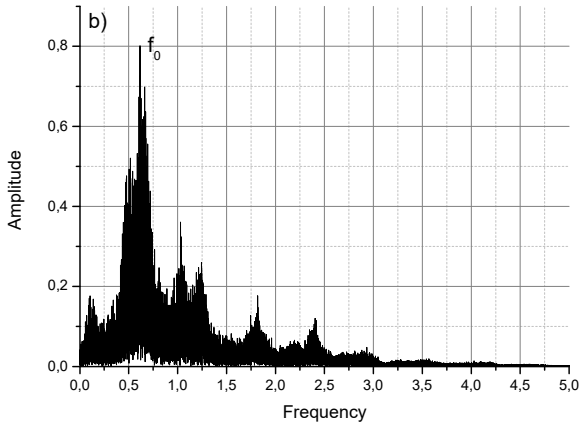
b)
f_0
Amplitude
Frequency
0,8
0,6
0,4
0,2
0,0
0,0
0,5
1,0
1,5
2,0
2,5
3,0
3,5
4,0
4,5
5,0